Thermohydrodynamic Modeling of a Tapered-Land Thrust Bearing with Validation Against Experimental Data

Seckin Gokaltun, Research Scientist, Member of ASME, Kingsbury, Inc.

Kingsbury, Inc.®
Over 100 Years of Bearing Innovation

Proceedings of ASME Turbo Expo 2021
Turbomachinery Technical Conference and Exposition
GT2021
June 7-11, 2021, Virtual, Online

GT2021-60203

THERMOHYDRODYNAMIC MODELING OF A TAPERED-LAND THRUST BEARING WITH VALIDATION AGAINST EXPERIMENTAL DATA

Seckin Gokaltun
Mechanical Research Engineer, Member of ASME
Kingsbury, Inc.
10385 Drummond Road
Philadelphia, Pennsylvania 19154
Email: sg@kingsbury.com

ABSTRACT

In this work, a computational fluid-film bearing analysis model has been utilized in order to investigate the conjugate heat transfer problem for a tapered-land bearing using computational fluid dynamics (CFD) analysis. The academic model is based on the 2D Reynolds equation for the pressure distribution in the film the 3D energy equation is solved for the the bearing pad and the fluid film; therefore, the lubricant properties such as viscosity and density could be made temperature-dependent. The runner is modeled using a 2D axisymmetric mesh. The current analysis excludes the mechanical or thermal deformations of the bearing and the runner since it was observed that the results for output quantities such as film temperature, film pressure, torque and load capacity were within reasonable agreement with the benchmark data obtained from the experiments for the majority of the speed and load cases studied. Comparisons of modeling results against the benchmark data was obtained for cases ranging from 2000 rpm to 10,000 rpm at loads varying from 1000 N to 8000 N. The importance of proper boundary conditions used in the heat transfer model is emphasized as well as the coupling of heat transfer between the film and the solid surfaces of collar and the bearing is described. The results obtained here yielded that a thermohydrodynamic (THD) model that includes the energy transfer into the structures surrounding the fluid film is sufficient enough to predict the performance of a tapered-land bearing at a wide speed and load range in the case where the runner is thick enough that the effect of deformations on the results can be ignored.

NOMENCLATURE

CFD Computational Fluid Dynamics
THD Thermohydrodynamic
TEHD Thermoelastohydrodynamic
h Film thickness
HP Power loss (hp)
M_t Friction torque
n Number of pads
P Static pressure
R_i Bearing inner radius
R_o Bearing outer radius
R_{ir} Runner inner radius
R_{or} Runner outer radius
T Temperature
W_p Pad thickness
W_1 Groove thickness
W_r Runner thickness
δ Taper height
ϕ_p Pad angle (degree)
ϕ_g Groove angle (degree)
ϕ_L Taper starting angle (degree)
ω Rotational speed (rpm)

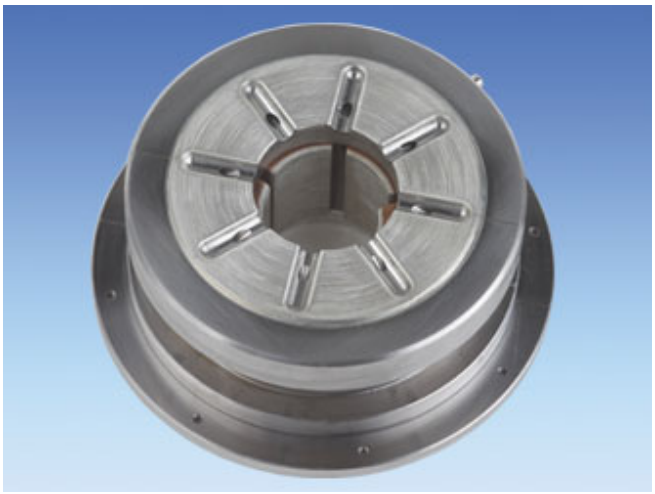

FIGURE 1: KINGSBURY'S HYDRODYNAMIC FIXED-PROFILE THRUST AND JOURNAL BEARING.

INTRODUCTION

Tapered-land thrust bearings are fluid-film bearings that fall into the category of fixed-profile thrust bearings among other designs such as flat-land thrust bearings, step-land thrust bearings and pocket–pad thrust bearings [1]. They share the common features of fixed-profile thrust bearings as they are simple to design and manufacture relative to more complex alternatives such as the tilting-pad thrust bearings. In comparison to other fixed-profile bearings, the tapered-land design allows to carry more load and can be utilized at a wider range of rotating speeds.

Tapered-land thrust bearings are mostly utilized in oil-lubricated rotating machinery such as turbines, pumps and turbochargers. They can be either used as a stand-alone bearing to support axial loads or combined with a journal bearing to constrain the radial orientation of the shaft as shown in Fig. 1. The thrust bearing pads are manufactured in the shape of circumferential sectors separated with grooves for fresh oil supply. The groove is provided with oil at the internal diameter of the bearing while the a much smaller exit area exists in the outer diameter of the groove to create a pocket for the fresh oil to mix with the hot oil leaving the pads. The tapered section of the thrust pad starts at the leading edge and usually spans majority of the pad angle where the pressure in the film would be developed due to the converging wedge. The taper is manufactured with a constant angle in circumferential direction or a compound taper could also be manufactured that spans both circumferential and radial directions. For bi-directional applications an opposite tapered section could also be machined at the trailing edge section of the thrust pads.

Prediction of the performance of tapered-land bearings is important to assess the operating limits based on the minimum film thickness and maximum pad temperature as well as evaluating power loss and oil flow requirements. One can refer to guides [2] and tables [3] published in the literature for quick design calculations. Booser et al. [4] have presented analytical expressions of temperature rise across the pads of a tapered-land bearing under laminar and turbulent conditions. It is also possible to utilize computer programs to obtain more detailed flow characteristics of the oil film as well as thermal and stress conditions on the bearing and collar structures. In one example of such an analysis, Brockett et al. [5] has used a Reynolds equation based film solver coupled with thermo-elastic deformation solver for the runner and the bearing in order to investigate the effect of runner deformations in the performance of a 6-in diameter, 10-pad tapered-land bearing. They have concluded that heat conduction into the bearing and the runner affected the results significantly especially at higher loads and consequently the thermal deformations played a more crucial role in predicting the pad temperatures compared to pure mechanical deformations. In a later study by Dadouche et al. [6] Reynolds equation based simulations were compared against experimental data for a 200 mm (7.87 in) tapered-land bearing [7] where only the heat conduction to the bearing was considered with an insulated collar assumption while the structural deformations were ignored. They concluded that only 10-20% of the heat was conducted to the bearing from the film and the relation of the maximum pad temperature to the oil inlet temperature wasn't linear.

A 3-inch tapered-land thrust bearing with inclined grooves was studied much earlier where water was used as the lubricant [8]. An isothermal Reynolds-equation based modeling was also conducted study the effect of the groove inclination angle and the effect of turbulence and centrifugal inertia. It was found that turbulence helped with the load capacity while inertia effects influenced the results less than 7%. The torque measurements obtained using a bearing with a 30° groove inclination angle showed a sharp change in the trend which indicated that the turbulence occured for maximum Reynolds number, $4100 < Re_{max} < 5000$. Recently Henry et al. [9] extended the speed range of the experiments of Dadouche [7] using a heavily instrumented, 89 mm (3.5 in) tapered-land thrust bearing and an upgraded experimental set-up. This study was selected as the benchmark case studied numerically in this work since detailed bearing performance characteristics were provided such as pad temperature, pressure, minimum film thickness and torque. A stiff collar was utilized to minimize the effect of mechanical deformations of the collar on the data collected.

In this work, we validate a computational model developed for thrust bearing analysis for the operating conditions published by University of Poitiers for a tapered-land thrust bearing. Figure 2 shows the range of load and surface speed studied by previous researchers experimentally and numerically. Compared to previous validation studies the current work extends the range of validation in terms of surface speed which covers the turbulent regime as well. Previous numerical investigations of tapered-

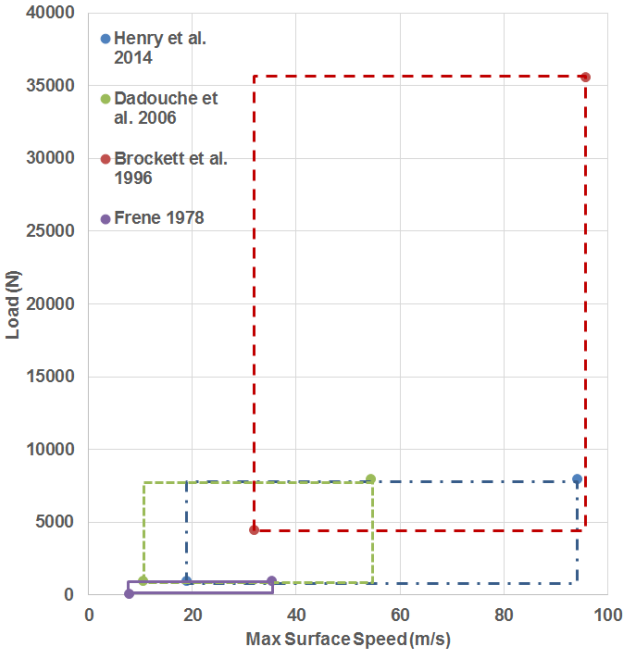

FIGURE 2: OPERATING CONDITIONS OF PREVIOUS WORKS CITED IN THE LITERATURE THAT STUDIED TAPERED-LAND THRUST BEARINGS.

land bearings were either not validated against experiments or comparisons were made for lower operating speeds.

The rest of the paper is organized as follows: first, the numerical model developed for modeling the tapered-land thrust bearing is shown. The geometry, material properties and boundary conditions are described. Next, the operating conditions of the bearing is presented and comparisons against experimental data is shown. Finally, conclusions and discussion of the analysis follow.

NUMERICAL MODEL

Governing Equations

The numerical model used in this work was built using THRUST v5.2 code developed by the Rotating Machinery and Controls Laboratory (ROMAC) of University of Virginia. It solves a two-dimensional Reynold's equation and the three-dimensional energy equation for the pressure and temperature distribution in the film, respectively. It also solves the heat conduction equation and the equations of elasticity for the bearing and the runner solid structures; however, the effect of deformations on bearing operation was assumed to be negligible in the current study. The generalized Reynold's equation is given as:

$$\frac{1}{r}\frac{\partial}{\partial r}\left(F_2 r\frac{\partial p}{\partial r}\right)+\frac{1}{r}\frac{\partial}{\partial \theta}\left(F_2\frac{1}{r}\frac{\partial p}{\partial \theta}\right)=\omega\frac{\partial}{\partial \theta}\left(\frac{F_1}{F_0}\right)-\dot{h}, \quad (1)$$

where

$$F_0=\int_0^h\frac{1}{\mu}dz, \quad F_1=\int_0^h\frac{z}{\mu}dz, \quad F_2=\int_0^h\frac{z^2}{\mu}dz-\frac{F_1^2}{F_0}. \quad (2)$$

Here, the film thickness, h, is expressed as below for a tapered land bearing with parallel taper leading and trailing edges:

$$h(r,\theta)=\begin{cases} h_0+\delta\left(1-\frac{r\sin\theta}{R_1\sin\phi_L}\right) & , \theta<\sin^{-1}\left(\frac{R_1}{r}\sin\phi_L\right) \\ h_0 & , \theta\geq\sin^{-1}\left(\frac{R_1}{r}\sin\phi_L\right)\end{cases}. \quad (3)$$

The energy solution in the film is obtained in three dimensions for an incompressible fluids with constant specific heat using the following equation where conduction terms in the circumferential and radial directions were also considered:

$$\begin{aligned}&\rho c_p\left[u_r\frac{\partial T}{\partial r}+\frac{u_\theta}{r}\frac{\partial T}{\partial \theta}+u_z\frac{\partial T}{\partial z}\right]= \\ &\frac{1}{r}\frac{\partial}{\partial r}\left[kr\frac{\partial T}{\partial r}\right]+\frac{1}{r^2}\frac{\partial}{\partial \theta}\left[k\frac{\partial T}{\partial \theta}\right]+\frac{\partial}{\partial z}\left[k\frac{\partial T}{\partial z}\right] \\ &+\mu\left[\left(\frac{\partial u_r}{\partial z}\right)^2+\left(\frac{\partial u_\theta}{\partial z}\right)^2\right].\end{aligned} \quad (4)$$

The Poisson's equation in three dimensions is given as $\nabla\cdot(\underline{k}\nabla T)+Q=0$ for the conduction of heat in the solid bodies which reduces to the three-dimensional Laplace's equation in Cartesian coordinates for a constant thermal conductivity, k, and zero internal heat generation, Q:

$$\frac{\partial^2 T}{\partial x^2}+\frac{\partial^2 T}{\partial y^2}+\frac{\partial^2 T}{\partial z^2}=0. \quad (5)$$

Additional details on the governing equations the THD code is based on can be found at [5] and [10].

Geometry and Boundary Conditions The bearing and the runner bodies included in the thermohydrodynamic analysis presented here are shown in Fig. 3. The triangular outlet cross section at the groove between the pads of the bearing and

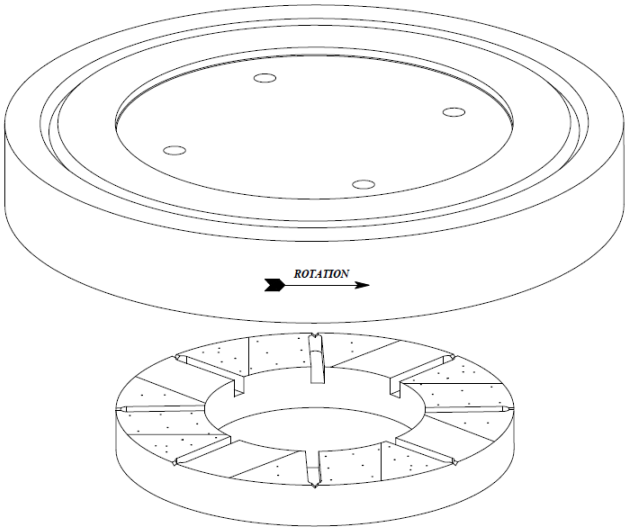

FIGURE 3: EXPERIMENTAL FIXED-PAD THRUST BEARING AND RUNNER INCLUDED IN THE THD MODEL.

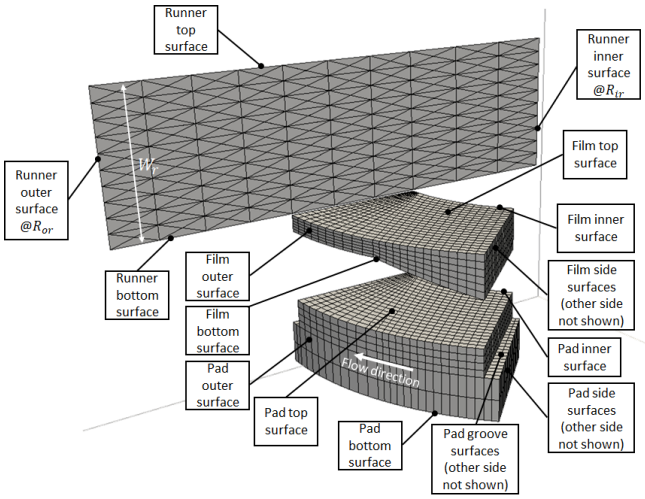

FIGURE 4: THE MESH REPRESENTING THE RUNNER, OIL FILM AND THE BEARING PAD IN THE THD ANALYSIS AND THE LABELING USED FOR THE BOUNDARY CONDITIONS.

the exact geometrical features on the shaft mounting side of the runner are not completely represented in the built-in geometry and mesh generator in the code; however, overall geometrical characteristics are captured well. The runner is represented as an axisymmetric two-dimensional slice in the radial direction with symmetry assumed in the circumferential direction while the three-dimensional bearing pad geometry and corresponding film layer are represented as sector cut models as shown in Fig. 4 with circumferential symmetry planes placed in the radial mid-planes of the grooves on each side of a bearing pad. The mesh for the oil film is exaggerated in size in the axial direction in Fig. 4 for better visualization of the tapered and the flat sections of the film.

Figure 5 shows the dimensions of one pad sector of the bearing geometry used in the code where the top layer of the mesh is scaled up for clarity here. The values used in the generation of the mesh is given in Table 1.

The boundary conditions at the film outer surface, film inner surface and film side surfaces are set so that the static pressure is equal to zero for the solution of the Reynold's equation. When the pressure drops below zero in areas of the film where cavitation is predicted then the pressure is assumed to be zero at those locations as well. Boundary conditions for the solution of the energy equation in the film include specified temperature values at the film top surface facing the runner and at the film bottom surface facing the bearing. The nodal temperatures at the interface surfaces are averaged and a constant temperature value is assigned to the film top surface at each iteration. On the other hand, the nodes in the film mesh at the film bottom surface are assigned pad temperature values at the same nodes that are shared with the

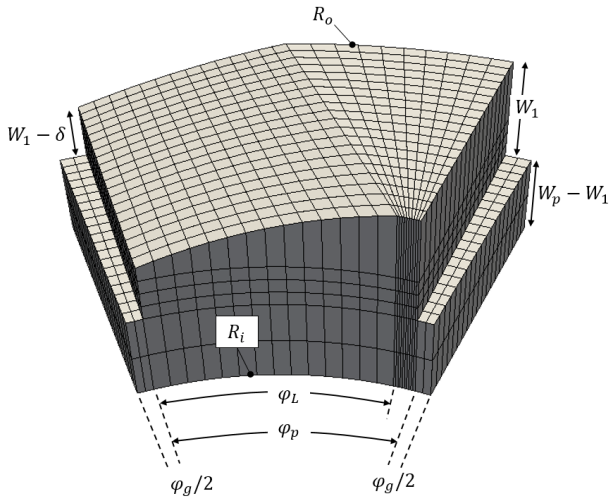

FIGURE 5: SIDE VIEW OF THE FEA MESH EXLUDING THE BASE RING.

pad mesh on pad top surface. The film outer surface, film inner surface and film trailing edge surface are assumed to be insulated while the film leading edge surface is assigned a constant temperature, T_i, based on the groove mixing model used in the code. There are various groove mixing models proposed in the literature but the version that is being used in this work uses the

TABLE 1: GEOMETRY DETAILS OF THE TAPERED-LAND BEARING AND THE RUNNER.

R_i	25 mm	R_{ir}	1 mm
R_o	45 mm	R_{or}	70 mm
W_p	10 mm	W_r	20 mm
W_1	4 mm	n	8
δ	0.0189 mm	ϕ_p	40°
ϕ_g	5°	ϕ_L	36.64°

following equation for the calculation of T_i:

$$T_i = T_f + \varepsilon \left(\frac{Q_s}{Q_i} - 1 \right) (T_f - T_o) \tag{6}$$

where $T_f = 40°$C is the oil supply temperature and T_o is the pad outlet film temperature and Q_i is the flow rate calculated at the pad leading edge while Q_s represents pad side leakage flow rate. This model is a variant of Neal's groove mixing model [11] where a hot-oil carry-over factor, ε, is utilized that represents the ratio of the hot oil from the preceding pad being unmixed with the fresh oil supply in the groove before it enters the pad at the leading edge. It is difficult to predict the value to use for the hot-oil carry-over factor and it usually depends on the bearing characteristics. In the results shown here a ratio of $\varepsilon = 1$ was used that matched the experimental data better.

The runner thermal boundary conditions include adiabatic conditions at the runner inner surface, a constant heat transfer coefficient value of $h_r = 25$ W/m^2.K with ambient temperature set at supply temperature $T_{r,\infty} = 40°$C at the runner top surface and runner outer surface. The film temperature at the interface with the runner was averaged and applied to the runner bottom surface as a fixed temperature boundary condition. The pad thermal boundary conditions include periodic symmetry at the pad side surfaces and a constant heat transfer coefficient value of $h_b = 1000$ W/m^2.K with ambient temperature set at $T_{b,\infty} = 40°$C at all other surrounding pad outer surfaces. The heat transfer coefficients and ambient temperatures used here are based on the previous computational fluid dynamics work by Charitopoulos et al. [12] where the effects of surface texturing was studied using the same benchmark bearing presented in this work. Although the heat transfer coefficients at other outer surfaces of the runner and bearing pad is provided in [12], only two values are utilized in this study since the THD code used in this work cannot specify individual heat transfer boundary conditions on each outer surface independently.

Material Properties The thrust bearing material used in the benchmark experimental case was bronze UE9P while the runner was of XC38 steel which is equivalent to AISI 1038. A thermal conductivity value of $k_b = 62 \times 10^{-3}$ kW/m.C for the bronze bearing and $k_r = 43.6 \times 10^{-3}$ kW/m.C for the steel runner were used.

The lubricant used in the benchmark experiments were ISO VG 46 mineral oil. Fluid properties, except viscosity, are used as non-temperature-dependent values. The specific gravity was selected to be $sg = 0.838$ using a density value of $\rho = 837.28$ kg/m^3 at $T = 77$ °C which corresponds to an average film temperature obtained in the experiments within the operating conditions studied in this work. The specific heat is calculated using the correlation $c_p = (1/sg@60°F^{0.5})(0.388 + 0.00045T)$ which yields 195.81 Btu.in/lbf.s^2-F at $T = 77°$ C which corresponds to $c_p = 2.1234$ kJ/kh.K. Similarly a fixed value, $k_f = 0.128$ kW/m.°C for the thermal conductivity was used that corresponded to $T = 77°$C.

The viscosity of the lubricant is represented as a function of temperature using the Roeland's viscosity-temperature-pressure equation as given below:

$$\mu_R = \mu_0 \exp\left\{ (\ln \mu_0 + 9.67) \left[\left(\frac{T - 138}{T_0 - 138} \right)^{-S_0} (1 + 5.1 \times 10^{-9} p)^Z - 1 \right] \right\} \tag{7}$$

where,

$$S_0 = -\frac{\ln \left[\frac{\ln \mu_1 / \mu_0}{\ln \mu_0 + 9.67} + 1 \right]}{\ln \left(\frac{T_1 - 138}{T_0 - 138} \right)} \tag{8}$$

and

$$Z = \frac{\ln \left[\frac{\ln \mu_2 / \mu_0}{\ln \mu_0 + 9.67} + 1 \right]}{\ln (1 + 5.1 \times 10^{-9} p_1)} \tag{9}$$

are termed as Roeland's thermoviscous and pressure-viscosity parameters, respectively [10]. In Eq.(7) T is in K, p is in Pa and μ is given in Pa.s. In this study, the pressure effects on viscosity was assumed to be negligible due to low film pressures so p in Eq.(7) is taken as zero. This is an assumption which could be taken when the additional viscosity value μ_2 at T_0 and p_1 is not known to calculate Eq.(9). Two viscosity values at two separate temperatures are needed to calculate the thermoviscous term for ISO VG 46 lubricant given in Eq.(8). Henry et al. [9] have reported that the lubricant used in the experiments had $\mu_0 = 0.0416$Pa.s at $T_0 = 40°$C and $\mu_1 = 0.0105$Pa.s at $T_1 = 80°$C which yields $S_0 = -1.16$. Figure 6 shows that Eq.(7) represents the temperature dependency of the dynamic viscosity of ISO VG 46 lubricant well.

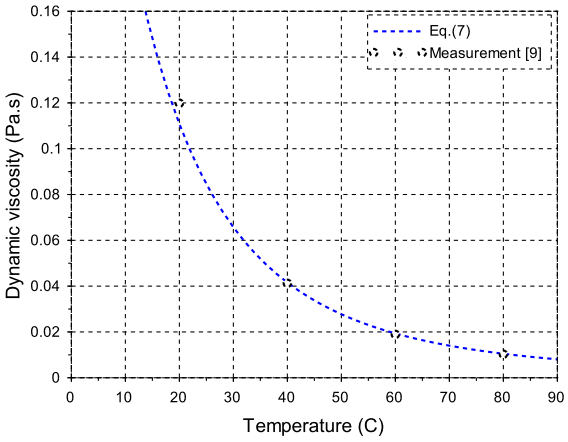

FIGURE 6: TEMPERATURE DEPENDENCY OF THE ISO VG 46 LUBRICANT USED IN THE CURRENT STUDY.

RESULTS

Simulations were conducted at 2000 rpm, 6000 rpm and 10,000 rpm rotational speeds which corresponds to 7.3 m/s, 21.9 m/s and 36.6 m/s linear velocity at mid radius, respectively. A set of eight nominal load conditions were calculated at each speed ranging from 1000 N to 8000 N at increments of 1000 N which resulted in an average pressure range of $0.25-2.04$ MPa. The inlet temperature for the lubricant was set at 40 C while the supply flow rate is not set in the code. The pressure was set at 0.1 MPa during the experiments in [9]; however, it is not available to specify inlet flow rate or supply pressure in the code used in this study for tapered-land bearings. Henry et al. [9] were able to vary inlet pressures from 0.05 MPa to 0.15 MPa at 40° C and have shown that the bearing performance in terms of minimum film thickness and friction torque was not affected significantly.

The flow is assumed to be laminar and the effect of cavitation is ignored. The maximum local Reynolds number calculated by the program was 167.6 which indicates the laminar flow assumption is valid.

The number of elements in the two-dimensional mesh for the solution of the Reynolds equation in the oil film was 480, while 400 elements were used in the asymmetric runner mesh. The number of elements in the 3D mesh used to solve the heat transfer was 2880 for the oil film and 3080 for the bearing pad. The mesh was refined for the film and the bearing pad consecutively twice as shown in Table 2 to evaluate the effect of the level of spatial discretization used in the results for temperature and pressure. Using the Richardson's extrapolation and grid convergence index method where the functionals chosen were the temperature at 75/75 location and pressure at 70/50 location at 8000 N and 6000 rpm, it was calculated that the uncertainty due to spatial discretization error at the base mesh level was less than 1% for both variables.

TABLE 2: EFFECT OF MESH REFINEMENT ON PRESSURE AND TEMPERATURE AT 75/75 LOCATION AND PRESSURE AT 70/50 LOCATION AT 6000 RPM AND 8000 N.

No. of elements	Base mesh	Fine mesh	Finer mesh
2D Reynolds eqn.	480	1080	1920
3D film energy eqn.	2880	6480	11520
3D pad energy eqn.	3080	9270	20640
75/75 temperature	84.22°C	83.77°C	83.55°C
70/50 pressure	3.538 MPa	3.511 MPa	3.499 MPa

Figure 7 shows the comparison of the pressure contours at the film-pad interface obtained at 8000 N for three different rotational speeds. The pictures on the top are THD results while the bottom figures are contour maps plotted using the experimental data. The contour plots that correspond to the experimental data has missing areas on the outer regions of the pad since measurements were not obtained at these locations. The peak pressure value is not captured in the experimental contour plots since the locations of the pressure taps on the surface of the pad don't correspond to the maximum pressure location. THD results indicate that with increased speed the peak pressure value drops which is expected as the film thickness gets larger. The location of the peak pressure is also observed to move towards the leading edge as the speed goes up. Experimental data indicates a shift of the peak location away from the land region of the pad while the drop in peak pressure with increased speed is not obvious as it is in the THD plots.

In addition to the 12 pressure taps shown in Fig. 7 the benchmark data is also available at the 70/50 location on the pad which corresponds to a point on the surface of the pad that is located at the radial centerline of the pad and 70% arc length distance away from the leading edge circumferentially. It is observed in Fig. 8 that the THD model is able to capture the static pressure on the surface of the pad at 70/50 location succesfully for the majority of the cases calculated at various loads. The relative percent error between the experimental data and the numerical results were calculated as $(P_{ROMAC}-P_{exp})/P_{exp}\times 100$. It was observed that for the cases where the load was larger than 3000 N the calculations are within 5% of the experimental pressure value at 70/50 location; however, the percent error at 1000 N ranges between 14% and 28% corresponding to speeds at 2000 rpm and 10000 rpm, respectively.

The 70/50 pressure value drops with increase in speed similarly as it was seen for peak pressures in Fig. 7 which is observed

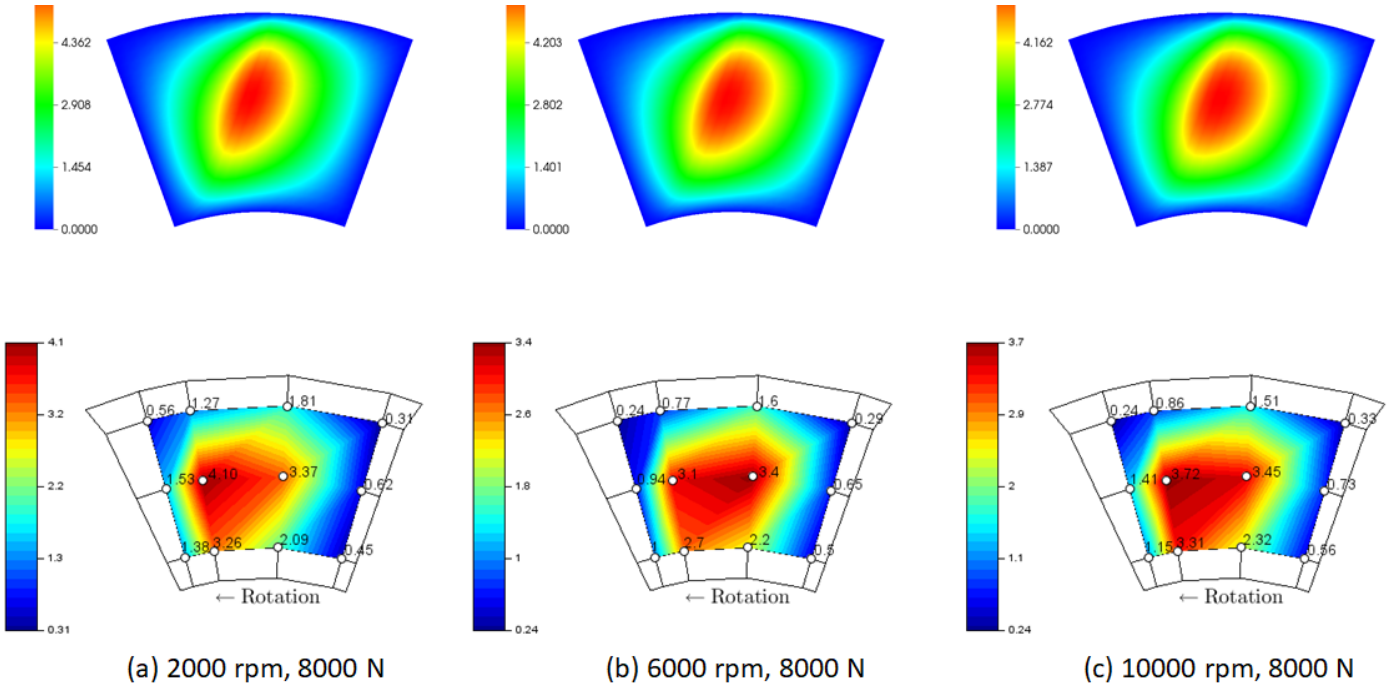

FIGURE 7: THD RESULTS (ON TOP) COMPARED AGAINST THE EXPERIMENTAL PRESSURE (UNITS IN *MPA*) PROFILES ALONG THE SURFACE OF THE PAD (ON THE BOTTOM) AT 8000 N.

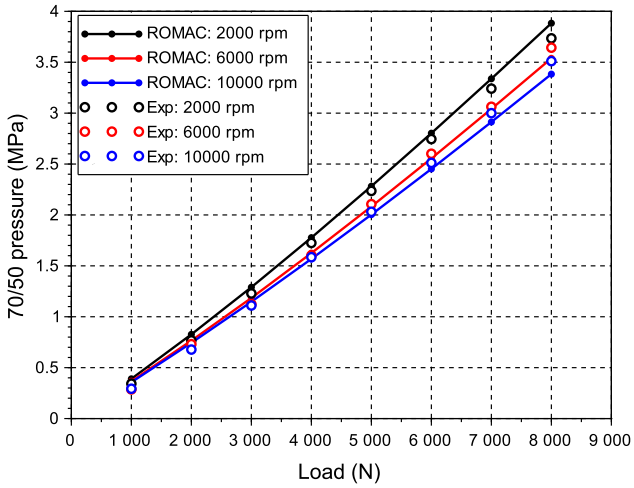

FIGURE 8: Comparison of ROMAC's THD results against the experimental data for average pad pressure at 70/50 location.

both in experimental data and THD results at all loads. It was observed that a five fold increase in speed (max surface speed 18.85 m/s to 94.25 m/s) doesn't correspond to a significant increase in the load capacity since the pressure distribution at 2000 N and 10,000 N are relatively similar in terms of peak pressure and profile.

The minimum pressure value is obtained as zero in the THD calculations as seen in Fig. 7 since zero pressure boundary condition was applied at the pad outer edges and negative film pressures predicted in the film are set to zero. It was also observed that the experimental measurements don't record pressure values lower than the atmospheric pressure at the 12 pressure points in the pad at any of the speeds analyzed in this work; therefore, it is concluded that cavitation effects are negligable in the calculations.

Film thickness measurements are also available from the benchmark data where two opposite proximity sensors attached to the bearing housing and facing the rotor were used. The comparison of the calculated minimum film thickness against the experimental data is shown in Fig. 9. It is observed that THD calculations without mechanical and thermal deformations were succesful in predicting the minimum film thickness among the load and speed range of the experiments. The percent error in film thickness was calculated to be within 10% of the experimental value for axial load less than 7000 N while the error raised up to 15% beyond that. One can think that the error is primarily related to the effect of mechanical and thermal deformations of the bear-

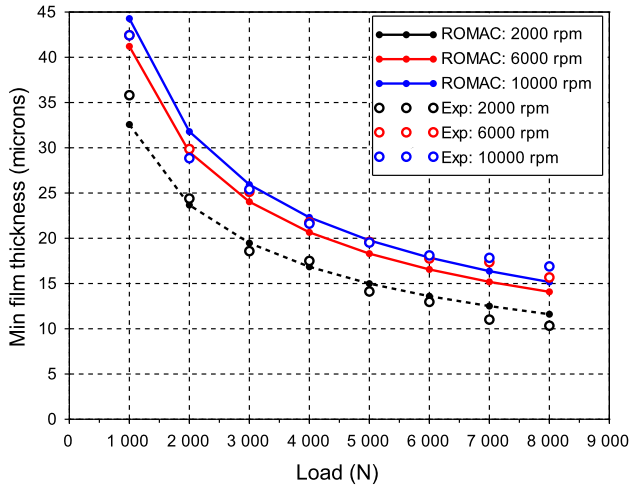

FIGURE 9: Comparison of ROMAC's THD results against the experimental data for minimum film thickness.

ing and collar that is ignored in the THD method. It is worth to note that the experimental measurements for the minimum film thickness don't account for the bearing deformations as the proximity probes are located outside the bearing. The experimental measurements include the collar deformations; however, the location of the sensors are outside of the film and that could have an error contribution to the experimental minimum film thickness values obtained.

Another contour plot comparison is presented in Fig. 10 for local temperature measurements on the pad surface for the calculated THD results against the experimental measurements at 8000 N for three rotational speeds at 2000 rpm, 6000 rpm and 10000 rpm. Similar to Fig. 7, the temperature maps obtained from the ROMAC code are shown on top at each speed while the contour plots for experimental temperature data are plotted on the bottom. As it was previously shown for the pressure contours, the parts of the pad where temperature measurements were not obtained are not included in the experimental temperature contour plots.

The THD results indicate a linear increase from the leading edge towards the trailing edge with the hottest point on the pad located at the corner on the land section of the pad at the outer diameter. This can be considered as an advantage of the tapered-land bearing design as the hottest pad surface point and the peak pressure point are not close to each other, which is considered to determine the ultimate load capacity of babbitted bearings in terms of creep behavior.

The linear change in temperature observed in the numerical results are also seen in the tapered section of the pad in the contour plots obtained from the experimental data. The temperature profile in the land section of the pad, on the other hand, shows an increase in temperature followed by a slight reduction getting close to the trailing edge of the pad. Consequently the hottest pad temperature doesn't occur at the point closest to the trailing edge top corner in the experimental temperature plots but slightly inward of the trailing edge. This difference in the temperature profiles is related to thermal crowning of the bearing pads and the collar which contributes to the error between the THD model and the benchmark data.

The percent error was calculated for the surface temperature calculated at the 75/75 location of the pad where the calculations were within 4% of experimental data for loads larger than 2000 N. At 1000 N the maximum percent error was 8%. Similar to the percent error calculated for the film pressure values at 70/50 location, the largest error for 75/75 film temperature also is observed at the lightest load studied in this work as shown in Fig. 11.

Possible sources of error in the calculations, besides ignoring the deformations, could be related to the limited surfaces on the mesh for the pad and runner where a heat transfer coefficient value can be assigned within the ROMAC code. The hot-oil carry-over factor has also a significant effect on the temperature comparison presented in Fig. 11. In this study 100% of the hot oil was assumed to be carried over to the next pad, hence the model slightly overpredicts the 75/75 temperatures as shown in Fig. 11 except at 2000 rpm. Finally the ROMAC code doesn't allow to specify an inlet pressure value for the lubricant supply which could also affect the sump temperature and the film temprature prediction at the leading edge of the pad.

Finally, the friction torque comparison is shown in Fig. 12 where the value of torque imposed on the runner by the fluid film is observed to increase with increasing load values. This is expected as the resistance in the film gets larger as the film thickness is reduced for higher loads. This value is directly related to the power loss due to viscous dissipation in the oil film. The ROMAC code calculates the power loss in the bearing by integrating the shear stress at the runner-film interface over the total bearing area and multiplying that with the moment arm with respect to the axis of rotation. The torque value is extracted from the power loss value output of the code using the relation, $HP = (2\pi M_t \omega / 396{,}000)$ which is then converted from hp to N.m by multiplying M_t with 0.1129848. The agreement between the THD calculation and the experimental values is reasonable where the relative percent error was calculated to be less than 10%.

CONCLUSIONS

In this paper, a computational analysis of a tapered-land bearing has been presented using ROMAC's Thrust code version 5.2. Pressure and temperature field in the film was calculated in conjunction with the solution of the heat conduction in

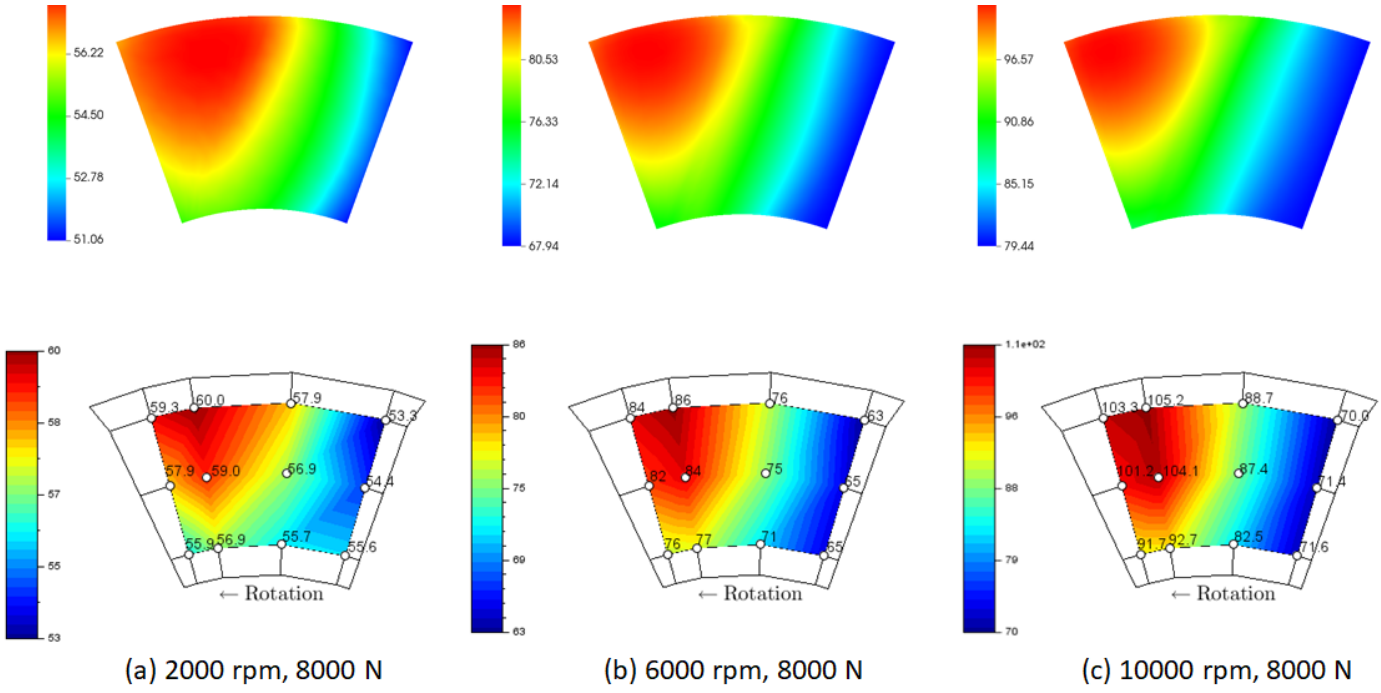

FIGURE 10: THD RESULTS (ON TOP) COMPARED AGAINST THE EXPERIMENTAL TEMPERATURE (UNITS IN *C*) PROFILES ALONG THE SURFACE OF THE PAD (ON THE BOTTOM) AT 8000 N.

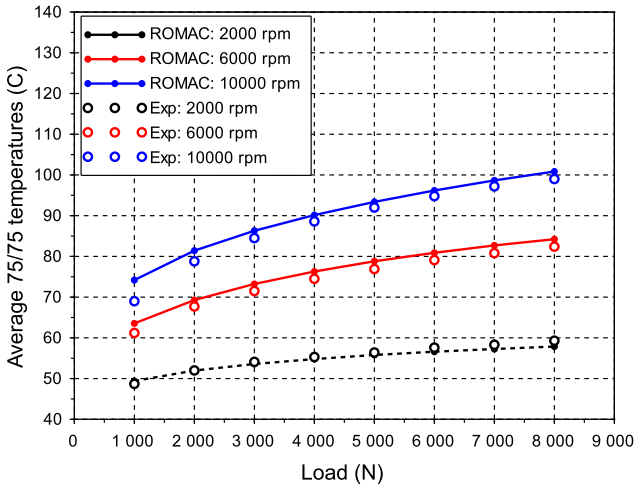

FIGURE 11: Comparison of ROMAC's THD results against the experimental data for average pad temperature at 75/75 location.

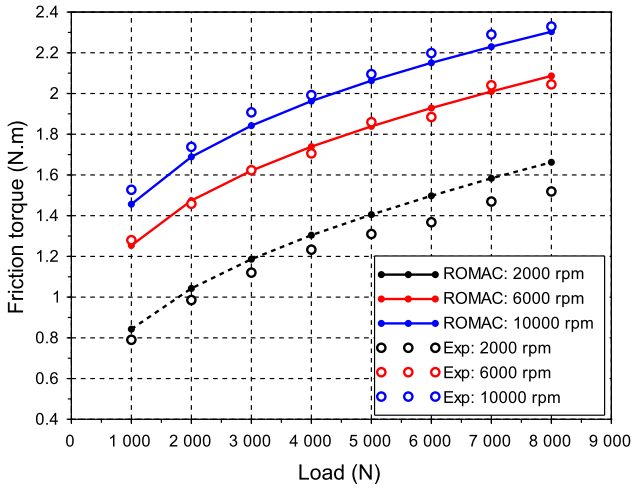

FIGURE 12: Comparison of ROMAC's THD results against the experimental data for friction torque.

the bearing pad and the runner structures on each side of the oil film. Although the mechanical and thermal deformations of the bearing and runner parts are not considered here, the calculations for pressure at 70/50 location on the pad surface, temperature value at 75/75 location, minimum film thickness and friction torque values were satisfactory. The most important inputs to the

computational model utilized here were observed to be the heat transfer coefficient values imposed as boundary condtions for the non-lubricated surfaces of the bearing and runner parts as well as the hot-oil carry-over factor. The correct selection of these parameters were instrumental in obtaining a good agreement between the calculations and the experimental data available from the benchmark problem that is modeled here.

Future work would include inclusion of the thermal and mechanical deformations in the calculations to evaluate if the error between the calculations and the experiments would get better especially for the comparison of temperature at 75/75 location. The Reynolds number calculated for the speed and load cases that were obtained from the experimental study was low enough to consider turbulence effects on the results; however, effect of cavitation would be important to include once the pad is allowed to crown thermally in future studies.

ACKNOWLEDGMENT

The author would like to thank the Kingsbury, Inc. for permission to publish this paper. Special thanks go to Prof. Michel Fillon who have provided the bearing geometry and information about the operating conditions used in this analysis. In addition, the authors would like to acknowledge the ROMAC lab at University of Virginia for providing the thrust bearing analysis code used in this study. Finally the author acknowledges his late mentor Scan DeCamillo for his contributions regarding the content of this paper and dedicates this work to his memory. Scan was an established expert in the field of fluid-film bearings with numerous publications and patents. He will be remembered as a legend in the bearing industry, and will be in our thoughts forever.

REFERENCES

[1] Dadouche, A., Fillon, M., and DeCamillo, S. M., 2013. "Hydrodynamic fixed geometry thrust bearings". *Encyclopedia of Tribology*, pp. 1718–1729.

[2] Raimondi, A., and Boyd, J., 1955. "Applying bearing theory to the analysis and design of pad-type bearings". *Trans. ASME,* ***77***(3), pp. 287–309.

[3] Khonsari, M., and Booser, E., 2008. "Applied tribology-lubrication and bearing design".

[4] Booser, E., Ryan, F., and CL, L., 1970. "Maximum temperature for hydrodynamic bearings under steady load". *Lubrication Engineering,* ***26***(7), p. 226.

[5] Brockett, T. S., Barrett, L. E., and Allaire, P. E., 1996. "Thermoelastohydrodynamic analysis of fixed geometry thrust bearings including runner deformation". *Tribology transactions,* ***39***(3), pp. 555–562.

[6] Dadouche, A., Fillon, M., and Dmochowski, W., 2006. "Performance of a hydrodynamic fixed geometry thrust bearing: comparison between experimental data and numerical results". *Tribology Transactions,* ***49***(3), pp. 419–426.

[7] Dadouche, A., Fillon, M., and Bligoud, J., 2000. "Experiments on thermal effects in a hydrodynamic thrust bearing". *Tribology international,* ***33***(3-4), pp. 167–174.

[8] Frene, J., 1978. "Tapered land thrust bearing operating in both laminar and turbulent regimes". *Asle Transactions,* ***21***(3), pp. 243–249.

[9] Henry, Y., Bouyer, J., and Fillon, M., 2014. "An experimental hydrodynamic thrust bearing device and its application to the study of a tapered-land thrust bearing". *Journal of Tribology,* ***136***(2), p. 021703.

[10] Brockett, T. S., 1996. "Thermoelastohydrodynamic lubrication in thrust bearings.". PhD thesis, University of Virginia, Charlottesville, VA.

[11] Neal, P., 1970. "Analysis of the taper-land bearing pad". *Journal of Mechanical Engineering Science,* ***12***(2), pp. 73–84.

[12] Charitopoulos, A., Fouflias, D., Papadopoulos, C., Kaiktsis, L., and Fillon, M., 2014. "Thermohydrodynamic analysis of a textured sector-pad thrust bearing: effects on mechanical deformations". *Mechanics & Industry,* ***15***(5), pp. 403–411.